Inference-Based Quantum Sensing

C. Huerta Alderete ,[1,2,3] Max Hunter Gordon ,[4,5] Frédéric Sauvage,[4] Akira Sone ,[6]
Andrew T. Sornborger ,[1,3] Patrick J. Coles,[4,3] and M. Cerezo [1,3,*]
[1]*Information Sciences, Los Alamos National Laboratory, Los Alamos, New Mexico 87545, USA*
[2]*Materials Physics and Applications Division, Los Alamos National Laboratory, Los Alamos, New Mexico 87545, USA*
[3]*Quantum Science Center, Oak Ridge, Tennessee 37931, USA*
[4]*Theoretical Division, Los Alamos National Laboratory, Los Alamos, New Mexico 87545, USA*
[5]*Instituto de Física Teórica, UAM/CSIC, Universidad Autónoma de Madrid, Madrid 28049, Spain*
[6]*Aliro Technologies, Inc, Boston, Massachusetts 02135, USA*

(Received 1 July 2022; revised 13 September 2022; accepted 3 October 2022; published 31 October 2022)

In a standard quantum sensing (QS) task one aims at estimating an unknown parameter θ, encoded into an n-qubit probe state, via measurements of the system. The success of this task hinges on the ability to correlate changes in the parameter to changes in the system response $\mathcal{R}(\theta)$ (i.e., changes in the measurement outcomes). For simple cases the form of $\mathcal{R}(\theta)$ is known, but the same cannot be said for realistic scenarios, as no general closed-form expression exists. In this Letter, we present an inference-based scheme for QS. We show that, for a general class of unitary families of encoding, $\mathcal{R}(\theta)$ can be fully characterized by only measuring the system response at $2n+1$ parameters. This allows us to infer the value of an unknown parameter given the measured response, as well as to determine the sensitivity of the scheme, which characterizes its overall performance. We show that inference error is, with high probability, smaller than δ, if one measures the system response with a number of shots that scales only as $\Omega(\log^3(n)/\delta^2)$. Furthermore, the framework presented can be broadly applied as it remains valid for arbitrary probe states and measurement schemes, and, even holds in the presence of quantum noise. We also discuss how to extend our results beyond unitary families. Finally, to showcase our method we implement it for a QS task on real quantum hardware, and in numerical simulations.

DOI: 10.1103/PhysRevLett.129.190501

Introduction.—Quantum sensing (QS) is one of the most promising applications for quantum technologies [1]. In QS experiments one uses a quantum system as a probe to interact with an environment. Then, by measuring the system, one aims at learning some relevant property of the environment (usually some characteristic parameter) with a precision and sensitivity that are higher than those achievable by any classical system [2]. QS has applications in a wide range of fields such as quantum magnetometry [3–6], thermometry [7–10], dark matter detection [11], and gravitational wave detection [12,13].

In a QS experiment one first prepares an n-qubit probe state ρ that is as sensitive as possible to an external parameter θ of interest. This ensures that upon encoding two distinct parameters θ and θ' on the system, the respective measurements associated to ρ_θ and $\rho_{\theta'}$ will be sufficiently distinguishable, a prerequisite to any task of sensing. Second, one obtains the system response $\mathcal{R}(\theta)$ to the external interaction by measuring some observable over ρ_θ. Third, if the functional form of $\mathcal{R}(\theta)$ is known and invertible, one can infer the value of θ from measurement outcomes, as well as estimate the sensitivity of the QS scheme.

In simple cases all the previous steps are well-characterized. For instance, in an idealized magnetometry experiment it is known that the optimal probe state is the n-qubit Greenberg-Horne-Zeilinger (GHZ) state, while the optimal measurement is a parity measurement [14,15]. In this case, $\mathcal{R}(\theta)=\cos(n\theta)$, which allows one to obtain the magnetic field as $\theta=\cos^{-1}[\mathcal{R}(\theta)]/n$ [assuming $\theta\in(-\pi/n,\pi/n)$], and the state's sensitivity as $(\Delta\theta)^2=1/n^2$, which corresponds to the Heisenberg limit [2]. However, the situation becomes more involved in realistic scenarios where the system dynamics are not known, and hence where the explicit functional form of $\mathcal{R}(\theta)$ may not be accessible. For instance, when noise in the magnetometry setting is taken into account, the GHZ state is no longer optimal [16–18]. In this case the true response $\mathcal{R}(\theta)$ will inevitably deviate from the idealized cosine formula, limiting the extent to which θ can be accurately estimated. While recent works have focused on maximizing the sensitivity of QS protocols in noisy situations, by means of variational approaches [17,19–24], methods to recover the true $\mathcal{R}(\theta)$ *in situ* are still lacking.

Here, we introduce a data-driven inference method that allows us to efficiently characterize the exact functional form of $\mathcal{R}(\theta)$ for a general class of unitary families. We show that $\mathcal{R}(\theta)$ can be expressed as a trigonometric polynomial of degree n, such that it can be fully determined

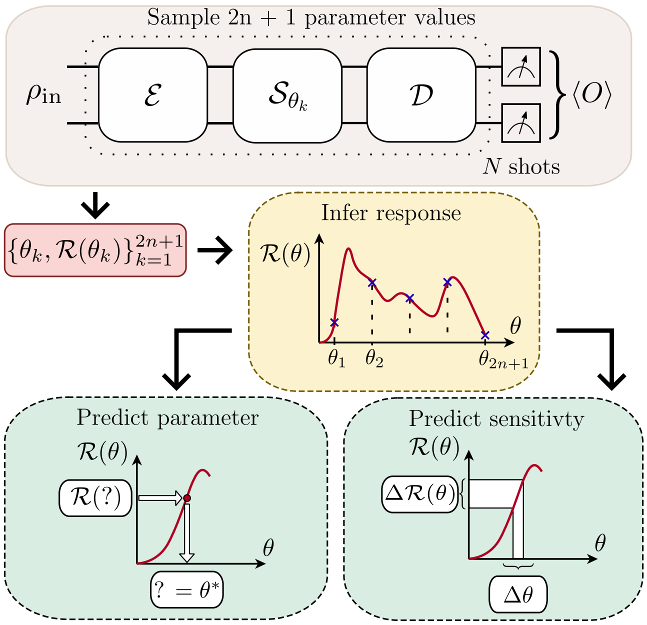

FIG. 1. Inference-based QS scheme. An input state ρ_{in} is sent through the following channels: state preparation $\mathcal{E}$, parameter encoding $\mathcal{S}_\theta$, premeasurement $\mathcal{D}$. We then measure the expectation value of O. By measuring the system response at $2n+1$ parameters, we can recover the exact form of $\mathcal{R}(\theta)$ in Eq. (3). From $\mathcal{R}(\theta)$ we can infer the value of a parameter given the system response, and compute the sensitivity of the sensing scheme.

by only measuring the system response at a set of $2n+1$ known parameters. We then discuss how the inferred function can be used to estimate the value of *any* unknown parameter, as well as the sensitivity of the scheme. Moreover, we rigorously analyze the inference error. Finally, we show that our method can be extended to cases where the system response is no longer exactly a trigonometric polynomial, but can still be approximated by one. The applications of the inference scheme are demonstrated in both numerical simulations as well as real implementations on a quantum computer.

Results.—Here, we consider a single-parameter QS setting employing an n-qubit probe state ρ to estimate a parameter θ. As shown in Fig. 1, ρ is prepared by sending a fiduciary state ρ_{in} through a state preparation channel $\mathcal{E}$ such that $\mathcal{E}(\rho_{\text{in}}) = \rho$. We focus on the case of unitary families where the parameter encoding mechanism is of the form

$$\mathcal{S}_\theta(\rho) = e^{-i\theta H/2}\rho\, e^{i\theta H/2} = \rho_\theta. \tag{1}$$

Here, H is a Hermitian operator such that $H = \sum_j h_j$ with $h_j^2 = \mathbb{1}$, and $[h_j, h_{j'}] = 0,\ \forall\ j,\ j'$. As shown below, the Hamiltonian in a magnetometry task is precisely of this form. We allow for the possibility of sending ρ_θ through a second premeasurement channel $\mathcal{D}$ that outputs an m-qubit state $\mathcal{D}(\rho_\theta)$ (with $m \leqslant n$), over which we measure the expectation value of an observable O, with $\|O\|_\infty \leqslant 1$. The system response is thus defined as

$$\mathcal{R}(\theta) = \mathrm{Tr}[\mathcal{D}\circ\mathcal{S}_\theta\circ\mathcal{E}(\rho_{\text{in}})O]. \tag{2}$$

This setting encompasses cases where $\mathcal{E}$ or $\mathcal{D}$ are noisy channels, as well as cases of imperfect parameter encoding where a θ-independent noise channel acts after $\mathcal{S}_\theta$, as is further discussed in the Supplemental Material (SM) [25].

Leveraging tools from the quantum machine learning literature [30] we prove the following theorem.

Theorem 1: Let $\mathcal{R}(\theta)$ be the response function in Eq. (2) for a unitary family as in Eq. (1). Then, for any $\mathcal{E}$, $\mathcal{D}$ and measurement operator O, $\mathcal{R}(\theta)$ can be exactly expressed as a trigonometric polynomial of degree n. That is,

$$\mathcal{R}(\theta) = \sum_{s=1}^{n} [a_s \cos(s\theta) + b_s \sin(s\theta)] + c, \tag{3}$$

with $\{a_s, b_s\}_{s=1}^n$ and c being real valued coefficients.

Notably, Theorem 1 determines the *exact* functional relation between the encoded parameter θ and the system response. Furthermore, the $2n+1$ coefficients $\{a_s, b_s\}_{s=1}^n$ and c, which are not known *a priori*, can be efficiently estimated by means of a trigonometric interpolation [31]. This is readily achieved by measuring the system responses at a set of predefined parameters $P = \{\theta_k\}_{k=1}^{2n+1}$ (see Fig. 1), as this leads to a system of $2n+1$ equations with $2n+1$ unknown variables. Hence, one needs to solve a linear system problem of the form $A\cdot\boldsymbol{x} = \boldsymbol{d}$. Here, $\boldsymbol{x} = [a_1, \ldots a_n, b_1, \ldots b_n, c]$ is the vector of unknown coefficients, $\boldsymbol{d} = [\mathcal{R}(\theta_1), \ldots, \mathcal{R}(\theta_{2n+1})]$ is a vector of measured system responses across P, and A is a $(2n+1)\times(2n+1)$ matrix with elements $A_{kj} = \cos(j\theta_k)$ for $j = 1, \ldots n$, $A_{kj} = \sin(j\theta_k)$ for $j = n+1, \ldots 2n$ and $A_{k(2n+1)} = 1$. Thus, solving $\boldsymbol{x} = A^{-1}\cdot\boldsymbol{d}$ allows us to fully characterize $\mathcal{R}(\theta)$. In the SM we provide additional details on this linear system problem.

Here, we note that A can be singular (for instance if $\theta_k = \theta_{k'} + 2\pi$ for any two $\theta_k, \theta_{k'} \in P$), and hence care must be taken when determining the $2n+1$ parameters. As shown in the SM, the optimal strategy is to uniformly sample the parameters as

$$\theta_k = \frac{2\pi(k-1)}{2n+1}, \quad \text{with} \quad k = 1, \ldots, 2n+1, \tag{4}$$

since this choice reduces the matrix inversion error.

In practice one cannot exactly evaluate the responses $\mathcal{R}(\theta_k)$, but rather can only estimate them up to some statistical uncertainty resulting from finite sampling. We define $\bar{\mathcal{R}}(\theta_k)$ as the N-shot estimate of $\mathcal{R}(\theta_k)$, and $\tilde{\mathcal{R}}(\theta)$ as the inferred response, a trigonometric polynomial of the form in Eq. (3), obtained by solving the linear system of equations with the estimates $\bar{\mathcal{R}}(\theta_k)$. The effect of the estimation errors on the accuracy of the inferred response can be rigorously quantified as follows.

Theorem 2: Let $\mathcal{R}(\theta)$ be the exact response function, and let $\tilde{\mathcal{R}}(\theta)$ be its approximation obtained from the N-shot estimates $\bar{\mathcal{R}}(\theta_k)$ with θ_k given by Eq. (4). Defining the maximum estimation error $\varepsilon = \max_{\theta_k \in P} |\mathcal{R}(\theta_k) - \bar{\mathcal{R}}(\theta_k)|$, then we have that for all θ

$$|\mathcal{R}(\theta) - \tilde{\mathcal{R}}(\theta)| \in \mathcal{O}(\varepsilon \log(n)). \tag{5}$$

Since the maximum estimation error ε is fundamentally related to the number of shots N, we can derive the following corollary.

Corollary 1: The number of shots N, necessary to ensure that with a (constant) high probability, and for all θ, the error $|\mathcal{R}(\theta) - \tilde{\mathcal{R}}(\theta)| \leqslant \delta$, for an inference error δ, is in $\Omega(\log^3(n)/\delta^2)$.

It follows from Corollary 1 that, for fixed δ, a polylogarithmic number of shots $N \in \Omega(\log^3(n))$ suffices to guarantee that $\tilde{\mathcal{R}}(\theta)$ will be a good approximation for the true response $\mathcal{R}(\theta)$. Once the inferred response is obtained, it can be further employed for tasks of parameter estimation and to characterize the sensitivity of a sensing apparatus—two aspects of central importance when devising a QS protocol (see Fig. 1).

When inferring the value of an unknown parameter θ', we assume that one is given an estimate of the system response $\bar{\mathcal{R}}(\theta')$, and the promise that θ' is sampled from a known domain Θ. In such a case, one estimates the unknown parameter as $\theta^* = \mathrm{argmin}_{\theta \in \Theta} |\tilde{\mathcal{R}}(\theta) - \bar{\mathcal{R}}(\theta')|$. In many cases of interest, such as high-precision estimation of small magnetic fields, Θ will be small enough such that $\tilde{\mathcal{R}}(\theta)$ is bijective, ensuring that the solution θ^* is unique. The resulting error in the estimate of the parameter θ' can be analyzed via the following corollary.

Corollary 2. Let ϵ' be the estimation error in $\bar{\mathcal{R}}(\theta')$ for some θ' in a known domain Θ where the system response is bijective. Let χ be the error introduced when estimating θ' via $\tilde{\mathcal{R}}(\theta)$ relative to the case when the exact response $\mathcal{R}(\theta)$ is used. The number of shots, N, necessary to ensure that with a (constant) high probability χ is no greater than δ' is $\Omega(\log^3(n)/(\delta' + \varepsilon')^2)$.

Corollary 2 certifies that $\tilde{\mathcal{R}}(\theta)$ can be used to infer an unknown parameter from a measured system response without incurring additional uncertainties as long as enough shots are used. In fact, for fixed δ' and ε', one only needs a polylogarithmic number of shots.

Our inference-based method also allows for estimating the sensitivity of QS schemes. Knowing the functional form of the response enables one to directly compute the sensitivity using the error propagation formula $(\Delta\theta)^2 = (\Delta\mathcal{R}(\theta))^2/|\partial_\theta \mathcal{R}(\theta)|^2$ [32,33], which relates the variance $(\Delta\theta)^2$ in estimates of the parameter θ to the variance $(\Delta\mathcal{R}(\theta))^2$ of the observable O used to estimate θ [i.e., $(\Delta\mathcal{R}(\theta))^2 = \mathrm{Tr}[\mathcal{D}\circ\mathcal{S}_\theta\circ\mathcal{E}(\rho_{\mathrm{in}})O^2] - \mathrm{Tr}[\mathcal{D}\circ\mathcal{S}_\theta\circ\mathcal{E}(\rho_{\mathrm{in}})O]^2$] and to the slope $\partial_\theta \mathcal{R}(\theta)$ of the response with respect to θ. When $O^2 = \mathbb{1}$ (i.e., measuring a Pauli operator), the sensitivity is

$$(\Delta\theta)^2 = \frac{1 - (\sum_{s=1}^{n} [a_s \cos(s\theta) + b_s \sin(s\theta)] + c)^2}{|\sum_{s=1}^{n} s[-a_s \sin(s\theta) + b_s \cos(s\theta)]|^2}. \tag{6}$$

A similar expression will hold when using $\tilde{\mathcal{R}}(\theta)$ in place of $\mathcal{R}(\theta)$. As shown in the SM, using $\tilde{\mathcal{R}}(\theta)$ to estimate the sensitivity at a parameter θ_l leads to an error that scales as $\mathcal{O}(\varepsilon \log(n)/D_l)$, where $D_l = \partial_\theta \mathcal{R}(\theta)|_{\theta=\theta_l}$. Moreover, as proven in the SM, a polynomial number of shots suffices to guarantee $|\Delta\theta - \Delta\tilde{\theta}| \leqslant \delta''$ for some fixed δ'' if $D_l \in \Omega(1/\mathrm{poly}(n))$. Notably, the inferred sensitivity $(\Delta\theta)^2$ in Eq. (6) can be compared with the quantum Cramer-Rao bounds [34,35], or the ultimate Heisenberg limit, to determine the optimality of the sensing scheme. In the SM we use this insight to show how our inferred response function can be used to train a measurement operator to reach the optimal sensing scheme given a fixed probe state.

One can further ask whether Eq. (3) can still be used in scenarios where the system response is no longer a trigonometric polynomial. Such a case will arise, for instance, if $\mathcal{S}_\theta$ is not of the form in Eq. (1). Still, we can leverage tools from trigonometric interpolation to accurately approximate the system response. Here, the following theorem holds for periodic responses and for parameters close enough to the θ_k values in P (regions of great interest for several QS tasks such as small magnetic field estimation).

Theorem 3: Let $f(\theta)$ be a 2π-periodic function with $|f(\theta)| \leqslant 1 \ \forall \ \theta$, and let $\tilde{\mathcal{R}}(\theta)$ be its trigonometric polynomial approximation obtained from the N-shot estimates of $\bar{f}(\theta_k)$, with θ_k given by Eq. (4). Defining the maximum estimation error $\varepsilon' = \max_{\theta_k \in P} |f(\theta_k) - \bar{f}(\theta_k)|$, and assuming that $|\theta - \theta_k| \in \mathcal{O}(1/\mathrm{poly}(n))$, then

$$|f(\theta) - \tilde{\mathcal{R}}(\theta)| \in \mathcal{O}\left(\max\left\{\frac{M}{\mathrm{poly}(n)}, \varepsilon' \log(n)\right\}\right), \tag{7}$$

where M is the Lipschitz constant of $f(\theta)$.

Theorem 3 shows that if $M \in \mathcal{O}(n)$, which can occur for a wide range of parameter encoding schemes [36], then we can derive a result similar to that in Corollary 1. Namely, using a polylogarithmic number of shots to estimate the quantities $\bar{f}(\theta_k)$ leads to $\tilde{\mathcal{R}}(\theta)$ being a good approximation of $f(\theta)$.

Experimental results.—We demonstrate the performance of the inference method for a magnetometry task performed on the IBM_MONTREAL quantum computer. This consists of preparing the GHZ state, encoding a magnetic field via

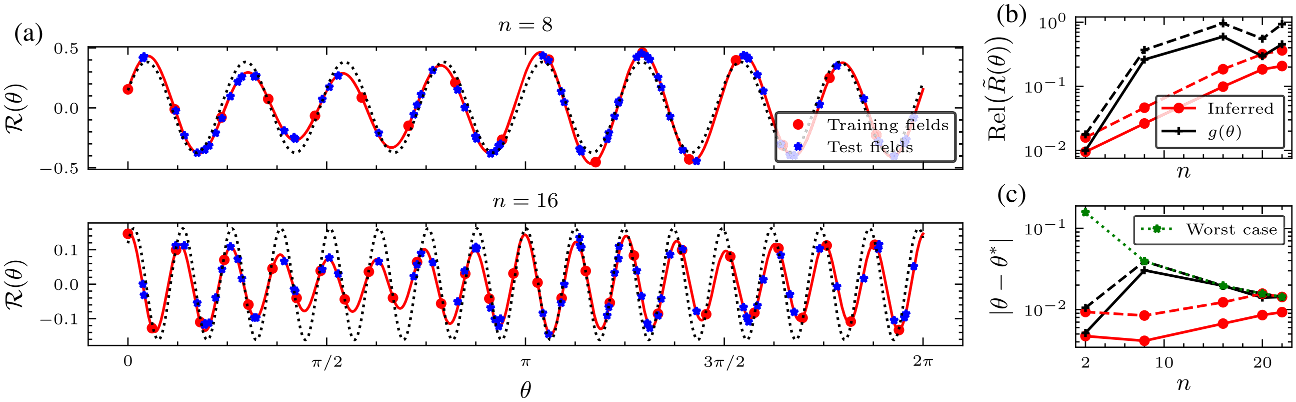

FIG. 2. Magnetometry task on IBM hardware. (a) Inferred response $\tilde{\mathcal{R}}(\theta)$ for system sizes of $n = 8$ and 16 qubits. The fields used to train (red point) and test (blue star) the inference scheme, were estimated on the IBM_MONTREAL quantum computer using 3.2×10^4 shots per expectation value. We depict the inferred response $\tilde{\mathcal{R}}(\theta)$ (red solid curve) as well as the fit $g(\theta) = \alpha \cos(\beta\theta + \gamma) + \zeta$ (black dotted curve). (b) Relative response error versus n. Statistics were obtained over 74 test fields and 7 experiment repetitions. The relative error is defined as the difference between the fit or inferred value and the measurement response, normalized by the average test expectation value. The red (black) points correspond to $\tilde{\mathcal{R}}(\theta)$ [$g(\theta)$], while solid (dashed) lines represent the median (upper quartile) error. (c) Parameter prediction error versus n, with green dots denoting the worst possible prediction (see SM).

Eq. (1) with $H = \sum_{j=1}^{n} Z_j$, and measuring the parity operator $O = \otimes_{j=1}^{n} X_j$. Here, Z_j and X_j are the Pauli z and x operators acting on the jth qubit, respectively. We set $\mathcal{D}$ to be the identity channel and perform the QS task for systems of up to $n = 22$ qubits.

We first measure the system response at $2n + 1$ training fields $\theta_k \in P$, sampled according to Eq. (4). These estimates are then used to infer the response $\tilde{\mathcal{R}}(\theta)$ of Eq. (3), as well as to fit a function $g(\theta) = \alpha \cos(\beta\theta + \gamma) + \zeta$. As discussed in the SM, the latter corresponds to a first order approximation of a noisy response under where the coefficients α, β, γ, and ζ correct the cosine to account for the effects of hardware noise. To evaluate the ability of these two functions to recover the true response of the system, we compare their predictions against the measured system response at a set of random test fields.

In Fig. 2(a) we display inference results for $n = 8$ and $n = 16$ qubits, indicating that our method (red solid curve) is clearly able to fit the training and test fields better than the cosine response (black dotted curve). More quantitatively, in Fig. 2(b), we show the scaling of the error as a function of the system size. One can see that for all problem sizes considered our method leads to smaller response prediction error. We note that for larger n the effect of noise becomes more prominent, as the hardware noise suppresses the measured expectation values [37–39]. Hence, in this regime both methods are equally limited by finite sampling noise that becomes of the same order as the magnitude of the response. Still, even for system sizes as large as $n = 22$ qubits, the inference method reduces the relative error by a factor larger than 2 when compared to that of the $g(\theta)$ fit. Finally, we also use $\tilde{\mathcal{R}}(\theta)$ and $g(\theta)$ for parameter estimation, i.e., to determine an unknown magnetic field encoded in the quantum state. As shown in Fig. 2(c), the $g(\theta)$ fit matches the worst possible prediction already for $n = 8$ qubits, whereas our inference method can outperform the $g(\theta)$ fit by up to 1 order of magnitude. In the SM we further discuss the behavior of the parameter prediction curves of Fig. 2(c).

Numerical simulations.—We complement the previous study with numerical results from a density matrix simulator that includes hardware noise, but where finite sampling can be omitted. We evaluate our inference method by emulating several magnetometry tasks as they would have been performed on a trapped-ion quantum computer (see [40,41]). To this end, we consider three different sensing setups. First, we study the same standard GHZ magnetometry setting as implemented on the IBM device. Second, we characterize the squeezing in a system where the probe state is a spin coherent state, $H = \sum_{j<k} X_j X_k$ is the one-axis twisting Hamiltonian [42], and $O = Z_n$ (note that we did not choose the optimal measurement operator $O = \sum_j Z_j$ as we want to showcase that we can infer the response for any choice of O). Finally, we study a scenario where the probe state is constructed by a unitary composed of four layers of a hardware efficient ansatz with random parameters [43,44], $H = \sum_{j=1}^{n-1} Z_j Z_{j+1}$ and $O = (1/n) \sum_{i=1}^{n} X_i$. (This case is relevant for variational quantum metrology [17,19,20,23,24], where one wishes to prepare a probe state via some parametrized quantum circuit that is usually initialized with random parameters.) In all cases $\mathcal{D}$ is the identity channel. See SM for further details, including the circuits employed.

As motivated by Corollary 1, $\tilde{\mathcal{R}}(\theta)$ is inferred with $N = \lceil 5 \times 10^2 \log(n)^2 \log[2 \times 10^2(2n + 1)] \rceil$ shots per θ_k. Figure 3(a) shows that in all three QS settings considered

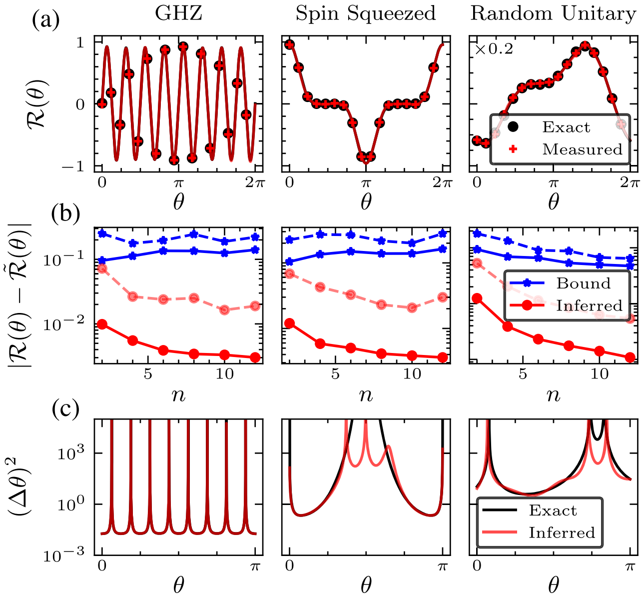

FIG. 3. Numerical results for QS tasks on a simulated noisy trapped ion device. (a) System response versus θ for $n = 8$ qubits in all three QS setups described in the main text. The exact response $\mathcal{R}(\theta)$ (black curve), and its value at the training fields $\mathcal{R}(\theta_k)$ (black points), were obtained with no finite sampling. In contrast, the response estimated at the training fields $\bar{\mathcal{R}}(\theta_k)$ (red crosses), and the resulting inferred function $\tilde{\mathcal{R}}(\theta)$ (red curve), were obtained with a polylogarithmic number of shots. (b) Median (solid) and maximum (dashed) of the error $|\mathcal{R}(\theta) - \tilde{\mathcal{R}}(\theta)|$ (red) and the bound of Theorem 2 (blue) for 10^4 test fields uniformly sampled over $(0, 2\pi)$. The statistics were obtained over 30 repetitions of the experimental setups. (c) Curves depict the inferred sensitivity versus θ. The exact (inferred) sensitivities are shown as a black (red) curves.

the inferred response closely matches the exact one [i.e., the red curve for $\tilde{\mathcal{R}}(\theta)$ and the black curve for $\mathcal{R}(\theta)$ are overlaid]. In Fig. 3(b) we further show the scaling of the error $|\mathcal{R}(\theta) - \tilde{\mathcal{R}}(\theta)|$ with respect to the system size. This analysis reveals that our method always performs significantly better than the upper bound given by Theorem 2. Indeed, we can see that allocating a number of shots N that increases polylogarithmically with n allows the error to decrease with increasing system size.

Finally, we use $\tilde{\mathcal{R}}(\theta)$ to estimate the sensitivity of the three experimental setups. As shown in Fig. 3(c), our method (red curves) recovers the behavior of the exact sensitivity (black curves). The sensitivity diverges in parameter regions where the experimental setup is insensitive to the field (when the response function has a vanishing gradient). In the SM we further provide a theoretical and numerical analysis for the estimated sensitivity, as well as the scaling of the error of inferring an unknown parameter.

Conclusions.—We introduced an inference-based scheme for QS that fully characterizes the response $\mathcal{R}(\theta)$ for a general class of unitary families by only measuring the system at $2n + 1$ known parameters. This framework leverages techniques from quantum machine learning and polynomial interpolation [30,45,46] for quantum sensing, leading to new insights and methodology for the characterization, implementation, and benchmarking of sensing protocols.

One of the main advantages of our method is that it can be readily combined with existing sensing protocols. For instance, further research could explore the use of the inferred response function in a variational setting, involving an optimization of the experimental setup to maximize the sensitivity and parameter prediction accuracy (see SM). This paves the way for a new approach in data-driven quantum machine learning for QS where the optimization procedure does not require knowledge of the classical or quantum Fisher information [17,20–24,47–52].

We thank Zoe Holmes, Michael Martin, and Michael McKerns for helpful and insightful discussions. C. H. A. and M. C. acknowledge support by NSEC Quantum Sensing at Los Alamos National Laboratory (LANL). M. H. G. was supported by the U.S. Department of Energy (DOE), Office of Science, Office of Advanced Scientific Computing Research, under the Quantum Computing Application Teams (QCAT) program. A. S. was supported by the internal R&D from Aliro Technologies, Inc. A. T. S., P. J. C., and M. C. were initially supported by the LANL ASC Beyond Moore's Law project. M. C. was supported by the LDRD program of LANL under Project No. 20210116DR. This work was also supported by the Quantum Science Center (QSC), a National Quantum Information Science Research Center of the U.S. Department of Energy (DOE). This research used quantum computing resources provided by the LANL Institutional Computing Program, which is supported by the U.S. DOE National Nuclear Security Administration under Contract No. 89233218CNA000001.

C. H. A and M. H. G. contributed to this work equally.

*Corresponding author.
cerezo@lanl.gov

[1] C. L. Degen, F. Reinhard, and P. Cappellaro, Quantum sensing, Rev. Mod. Phys. **89**, 035002 (2017).

[2] Vittorio Giovannetti, Seth Lloyd, and Lorenzo Maccone, Quantum Metrology, Phys. Rev. Lett. **96**, 010401 (2006).

[3] Jacob M. Taylor, Paola Cappellaro, Lilian Childress, Liang Jiang, Dmitry Budker, P. R. Hemmer, Amir Yacoby, Ronald Walsworth, and M. D. Lukin, High-sensitivity diamond magnetometer with nanoscale resolution, Nat. Phys. **4**, 810 (2008).

[4] Sourav Bhattacharjee, Utso Bhattacharya, Wolfgang Niedenzu, Victor Mukherjee, and Amit Dutta, Quantum magnetometry using two-stroke thermal machines, New J. Phys. **22**, 013024 (2020).

[5] John F. Barry, Matthew J. Turner, Jennifer M. Schloss, David R. Glenn, Yuyu Song, Mikhail D. Lukin, Hongkun Park, and Ronald L. Walsworth, Optical magnetic detection of single-neuron action potentials using quantum defects in diamond, Proc. Natl. Acad. Sci. U.S.A. **113**, 14133 (2016).

[6] Francesco Casola, Toeno Van Der Sar, and Amir Yacoby, Probing condensed matter physics with magnetometry based on nitrogen-vacancy centres in diamond, Nat. Rev. Mater. **3**, 17088 (2018).

[7] Luis A Correa, Mohammad Mehboudi, Gerardo Adesso, and Anna Sanpera, Individual Quantum Probes for Optimal Thermometry, Phys. Rev. Lett. **114**, 220405 (2015).

[8] Antonella De Pasquale, Davide Rossini, Rosario Fazio, and Vittorio Giovannetti, Local quantum thermal susceptibility, Nat. Commun. **7**, 12782 (2016).

[9] Akira Sone, Quntao Zhuang, and Paola Cappellaro, Quantifying precision loss in local quantum thermometry via diagonal discord, Phys. Rev. A **98**, 012115 (2018).

[10] Akira Sone, Quntao Zhuang, Changhao Li, Yi-Xiang Liu, and Paola Cappellaro, Nonclassical correlations for quantum metrology in thermal equilibrium, Phys. Rev. A **99**, 052318 (2019).

[11] Surjeet Rajendran, Nicholas Zobrist, Alexander O. Sushkov, Ronald Walsworth, and Mikhail Lukin, A method for directional detection of dark matter using spectroscopy of crystal defects, Phys. Rev. D **96**, 035009 (2017).

[12] L. McCuller, C. Whittle, D. Ganapathy, K. Komori, M. Tse, A. Fernandez-Galiana, L. Barsotti, P. Fritschel, M. MacInnis, F. Matichard *et al.*, Frequency-Dependent Squeezing for Advanced LIGO, Phys. Rev. Lett. **124**, 171102 (2020).

[13] M. e Tse, Haocun Yu, Nutsinee Kijbunchoo, A. Fernandez-Galiana, P. Dupej, L. Barsotti, C. D. Blair, D. D. Brown, S. E. Dwyer, A. Effler *et al.*, Quantum-Enhanced Advanced LIGO Detectors in the Era of Gravitational-Wave Astronomy, Phys. Rev. Lett. **123**, 231107 (2019).

[14] Daniel M. Greenberger, Michael A. Horne, Abner Shimony, and Anton Zeilinger, Bell's theorem without inequalities, Am. J. Phys. **58**, 1131 (1990).

[15] D. Leibfried, M. D. Barrett, T. Schaetz, J. Britton, J. Chiaverini, W. M. Itano, J. D. Jost, C. Langer, and D. J. Wineland, Toward Heisenberg-limited spectroscopy with multiparticle entangled states, Science **304**, 1476 (2004).

[16] Susanna F. Huelga, Chiara Macchiavello, Thomas Pellizzari, Artur K. Ekert, Martin B. Plenio, and J. Ignacio Cirac, Improvement of Frequency Standards with Quantum Entanglement, Phys. Rev. Lett. **79**, 3865 (1997).

[17] Bálint Koczor, Suguru Endo, Tyson Jones, Yuichiro Matsuzaki, and Simon C. Benjamin, Variational-state quantum metrology, New J. Phys. **22**, 083038 (2020).

[18] Lukas J. Fiderer, Julien M. E. Fraïsse, and Daniel Braun, Maximal Quantum Fisher Information for Mixed States, Phys. Rev. Lett. **123**, 250502 (2019).

[19] M. Cerezo, Andrew Arrasmith, Ryan Babbush, Simon C. Benjamin, Suguru Endo, Keisuke Fujii, Jarrod R. McClean, Kosuke Mitarai, Xiao Yuan, Lukasz Cincio, and Patrick J. Coles, Variational quantum algorithms, Nat. Rev. Phys. **3**, 625 (2021).

[20] Jacob L. Beckey, M. Cerezo, Akira Sone, and Patrick J. Coles, Variational quantum algorithm for estimating the quantum Fisher information, Phys. Rev. Res. **4**, 013083 (2022).

[21] Akira Sone, M. Cerezo, Jacob L. Beckey, and Patrick J. Coles, A generalized measure of quantum Fisher information, Phys. Rev. A **104**, 062602 (2021).

[22] M. Cerezo, Akira Sone, Jacob L. Beckey, and Patrick J. Coles, Sub-quantum Fisher information, Quantum Sci. Technol. **6**, 035008 (2021).

[23] Raphael Kaubruegger, Denis V. Vasilyev, Marius Schulte, Klemens Hammerer, and Peter Zoller, Quantum Variational Optimization of Ramsey Interferometry and Atomic Clocks, Phys. Rev. X **11**, 041045 (2021).

[24] Johannes Jakob Meyer, Johannes Borregaard, and Jens Eisert, A variational toolbox for quantum multi-parameter estimation, npj Quantum Inf. **7**, 89 (2021).

[25] See Supplemental Material at http://link.aps.org/supplemental/10.1103/PhysRevLett.129.190501, which contains additional details and proofs as well as Refs. [26–29].

[26] Y. P. Hong and C.-T. Pan, A lower bound for the smallest singular value, Linear Algebra Appl. **172**, 27 (1992).

[27] Roger A. Horn and Charles R. Johnson, *Topics in Matrix Analysis* (Cambridge University Press, Cambridge, England, 1991).

[28] Dunham Jackson, On the accuracy of trigonometric interpolation, Trans. Am. Math. Soc. **14**, 453 (1913).

[29] Knut Petras, Error estimates for trigonometric interpolation of periodic functions in lip 1, Ser. Approximations Decompositions **6**, 459 (1995), https://citeseerx.ist.psu.edu/viewdoc/download?doi=10.1.1.34.2151&rep=rep1&type=pdf.

[30] Ken M. Nakanishi, Keisuke Fujii, and Synge Todo, Sequential minimal optimization for quantum-classical hybrid algorithms, Phys. Rev. Res. **2**, 043158 (2020).

[31] Antoni Zygmund, *Trigonometric Series* (Cambridge University Press, Cambridge, England, 2002), Vol. 1.

[32] Luca Pezzè, Augusto Smerzi, Markus K. Oberthaler, Roman Schmied, and Philipp Treutlein, Quantum metrology with nonclassical states of atomic ensembles, Rev. Mod. Phys. **90**, 035005 (2018).

[33] Jasminder S. Sidhu and Pieter Kok, Geometric perspective on quantum parameter estimation, AVS Quantum Sci. **2**, 014701 (2020).

[34] Masahito Hayashi, *Quantum Information Theory: Mathematical Foundation (2nd edition)* (Springer, New York, 2004).

[35] Jing Liu, Jie Chen, Xiao-Xing Jing, and Xiaoguang Wang, Quantum Fisher information and symmetric logarithmic derivative via anti-commutators, J. Phys. A **49**, 275302 (2016).

[36] Ryan Sweke, Frederik Wilde, Johannes Jakob Meyer, Maria Schuld, Paul K. Fährmann, Barthélémy Meynard-Piganeau, and Jens Eisert, Stochastic gradient descent for hybrid quantum-classical optimization, Quantum **4**, 314 (2020).

[37] Samson Wang, Enrico Fontana, M. Cerezo, Kunal Sharma, Akira Sone, Lukasz Cincio, and Patrick J. Coles, Noise-induced barren plateaus in variational quantum algorithms, Nat. Commun. **12**, 6961 (2021).

[38] Daniel Stilck França and Raul Garcia-Patron, Limitations of optimization algorithms on noisy quantum devices, Nat. Phys. **17**, 1221 (2021).

[39] Samson Wang, Piotr Czarnik, Andrew Arrasmith, M. Cerezo, Lukasz Cincio, and Patrick J. Coles, Can error mitigation improve trainability of noisy variational quantum algorithms? arXiv:2109.01051.

[40] Lukasz Cincio, Yiğit Subaşı, Andrew T. Sornborger, and Patrick J. Coles, Learning the quantum algorithm for state overlap, New J. Phys. **20**, 113022 (2018).

[41] Colin J. Trout, Muyuan Li, Mauricio Gutiérrez, Yukai Wu, Sheng-Tao Wang, Luming Duan, and Kenneth R. Brown, Simulating the performance of a distance-3 surface code in a linear ion trap, New J. Phys. **20**, 043038 (2018).

[42] Masahiro Kitagawa and Masahito Ueda, Squeezed spin states, Phys. Rev. A **47**, 5138 (1993).

[43] Abhinav Kandala, Antonio Mezzacapo, Kristan Temme, Maika Takita, Markus Brink, Jerry M. Chow, and Jay M. Gambetta, Hardware-efficient variational quantum eigensolver for small molecules and quantum magnets, Nature (London) **549**, 242 (2017).

[44] M. Cerezo, Akira Sone, Tyler Volkoff, Lukasz Cincio, and Patrick J. Coles, Cost function dependent barren plateaus in shallow parametrized quantum circuits, Nat. Commun. **12**, 1791 (2021).

[45] Olivia Di Matteo, Josh Izaac, Tom Bromley, Anthony Hayes, Christina Lee, Maria Schuld, Antal Száva, Chase Roberts, and Nathan Killoran, Quantum computing with differentiable quantum transforms, arXiv:2202.13414.

[46] David Wierichs, Josh Izaac, Cody Wang, and Cedric Yen-Yu Lin, General parameter-shift rules for quantum gradients, Quantum **6**, 677 (2022).

[47] Johannes Jakob Meyer, Fisher information in noisy intermediate-scale quantum applications, Quantum **5**, 539 (2021).

[48] Iris Cong, Soonwon Choi, and Mikhail D. Lukin, Quantum convolutional neural networks, Nat. Phys. **15**, 1273 (2019).

[49] Arthur Pesah, M. Cerezo, Samson Wang, Tyler Volkoff, Andrew T. Sornborger, and Patrick J. Coles, Absence of Barren Plateaus in Quantum Convolutional Neural Networks, Phys. Rev. X **11**, 041011 (2021).

[50] Kunal Sharma, M. Cerezo, Lukasz Cincio, and Patrick J. Coles, Trainability of Dissipative Perceptron-Based Quantum Neural Networks, Phys. Rev. Lett. **128**, 180505 (2022).

[51] Jeffrey Marshall, Filip Wudarski, Stuart Hadfield, and Tad Hogg, Characterizing local noise in QAOA circuits, IOP SciNotes **1**, 025208 (2020).

[52] Cheng Xue, Zhao-Yun Chen, Yu-Chun Wu, and Guo-Ping Guo, Effects of quantum noise on quantum approximate optimization algorithm, Chin. Phys. Lett. **38**, 030302 (2021).